ISSN: 2633-4828 Vol. 5 No. S4, (July-Aug 2023)

International Journal of Applied Engineering & Technology

THE EFFECT OF THE INITIAL TEMPERATURE OF A COOLING PLATE ON TEMPERATURE DISTRIBUTION PATTERNS AND HEAT TRANSFER

Narongsak Kumphan[1], Suradet Tantrairatn[2], Watcharapong Patangtalo[3], Pasada Yisunzam[4*]

[1,2,3] Suranaree University of Technology, Nakhon Ratchasima, Thailand

[4] Khon Kaen University, Khon Kaen, Thailand, Thailand

[1] narongsakkumphan.sut@gmail.com, [2]suradetj@sut.ac.th, [3] watcharapong@sut.ac.th, [4] unchisay@kkumail.com

Abstract

This research focuses on designing cooling plates with internal channels to study and compare the temperature distribution at various positions and surface levels. Using Ansys Transient Thermal for the simulation, the cooling plate size is set at 180x180 mm with a thickness of 13 mm, made of aluminium. The plate features 14 channels, and the heat transfer coefficient (h) within these channels is varied between 3000 and 4200 W/m^2K at initial temperatures of 40, 50, 60, and 70°C. The findings indicate that a higher h results in better heat transfer and temperature distribution than a lower h. At higher initial temperatures, the heat transfer becomes similar regardless of the h value. The temperature distribution trend is consistent across the different surface levels of the aluminium plate.

Keywords*: Cooling Plate, Heat Exchanger, Channel Flow, Enhanced Heat Transfer.*

INTRODUCTION

In today's world, electric cars represent a significant innovation reshaping the automotive industry. This transformation is driven by a growing awareness of pressing environmental issues and the need to reduce greenhouse gas emissions. Electric cars offer a sustainable alternative to traditional internal combustion engine vehicles. The advancement of battery technology and the development of charging infrastructure have made electric cars an efficient and cost-effective option for consumers worldwide. A critical component of electric cars is the battery, which can be likened to the primary power source. The lifespan of an electric car depends on the performance of its battery. If the battery temperature exceeds a certain threshold, it can lead to a decrease in battery performance.

Therefore, batteries must incorporate an efficient cooling system. The optimal operating temperature for lithium-ion batteries typically ranges between 20 and 60 degrees Celsius. To ensure safety and performance, batteries must have an effective cooling system. The suitable operating temperature for lithium-ion batteries typically ranges between 20 and 60 degrees Celsius. If the battery temperature rises too high, it can lead to a decrease in battery performance. Therefore, batteries must incorporate an efficient cooling system. The optimal operating temperature for lithium-ion batteries typically ranges between 20 and 60 degrees Celsius. [1,2] One concern in battery technology, especially lithium-ion batteries widely used in electric cars, is the risk of thermal runaway. This occurs when the battery rapidly heats up and cannot be controlled, leading to potentially dangerous situations like fires or explosions.

High temperatures can result from various factors, such as faulty charging or discharging, physical damage to the battery, or defects in battery management systems. Therefore, this phenomenon is termed "thermal runaway." [3-7] The cooling system that dissipates heat from the battery comprises two main types: air cooling systems [8-11] and liquid cooling systems. The cooling system utilizing liquid [12-17] and phase change material (PCM) [18-22] for dissipating heat is widely employed. Liquid cooling systems are popular due to their efficient heat dissipation, ensuring widespread acceptance. Zihan Chen et al. [23] investigated a dual-layer liquid cooling plate inspired by the leaf structure of plants. In this design, the upper flow channels of the cooling plate contact the battery module for heat exchange.

In contrast, the lower flow channels reinforce the uncovered areas to ensure uniform heat distribution throughout the module. Ping He et al. [24] enhanced the temperature performance of lithium-ion batteries in vehicles by designing a two-layer liquid cooling plate, where the upper channels use coolant to dissipate heat, and the lower channels are used to recover the coolant. Ding Zhao et al. [25] designed a honeycomb structure liquid cooling plate (HLCP) to increase the heat exchange area of the liquid cooling plate (LCP) channels, thereby improving the heat dissipation efficiency of the LCP. Dense honeycomb channels significantly increase the heat exchange area of the heat dissipation channels. Kumar Kirad et al. [26] considered the appropriate parameter values of the battery module spacing, where changes in spacing length and width between batteries affect heat dissipation efficiency. Cong Wang et al. [27] introduced a novel liquid cooling system design with four cooling channels for immersion lithium-ion batteries using silicon heat dissipation sheets. The flow direction has no impact on heat dissipation.

Additionally, they discussed the efficient heat dissipation of liquid-cooled systems for discharge rates of 3C and 5C. Yubai Li et al. [27] developed a three-dimensional (3D) heat model comprising 14 prismatic batteries under rapid charge and abnormal usage conditions. When the cooling agent flow rate is low, cell temperature rapidly increases. This detailed 3D model provides in-depth data to prevent thermal runaway. Wei Kong et al. [28] designed various heat dissipation plates (TOCP, CCCP, SCCP). For CCCP, direct channels reduce the heat exchange area between the coolant and the cooling plate. They also discussed temperature differences and flow rates of different cooling agents.

Past research has shown the importance of effectively dissipating heat from batteries. Thus, this study aims to compare heat dissipation plate designs with and without channels. The ANSYS TRANSIENT program simulates heat dissipation as battery temperatures range from 40 to 70 degrees Celsius. The goal is to analyze temperature distribution within the plates and heat transfer, providing insights for channel design.

METHODOLOGY

In studying a cooling plate's temperature distribution and heat transfer, the Ansys transient thermal program is utilized to develop a model. The model aims to simulate the behaviour of the plate, as depicted in Figure 1. In Figure 1(a), the cooling plate is shown as a plain plate, while in Figure 1(b), it is compared with a cooling plate featuring channels. The cooling plate is a square with dimensions of 180x180 millimetres and a thickness of 13 millimetres. The primary objective is to analyze temperature fluctuations within the plate, with a particular focus on the scenario of a cooling plate with channels, as illustrated in Figure 2

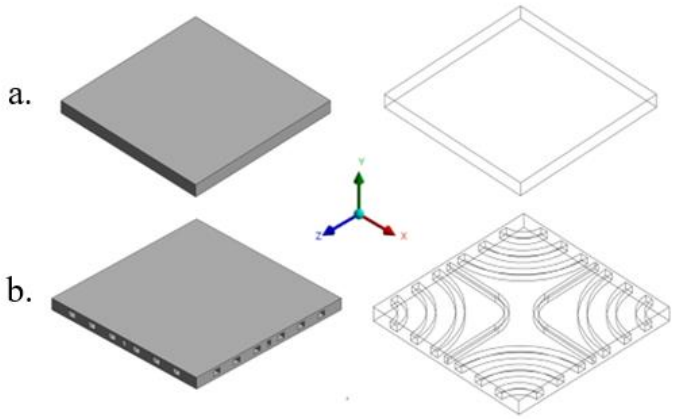

Figure 1 Geometry a) cooling plate b) cooling plate with channel

The cooling plate depicted in Figure 2 and Figure 3 features 14 channels, comprising 12 larger and two smaller channels. The dimensions of the larger channels are rectangular, measuring 6x8 millimetres, while the smaller channels measure 4x6 millimetres. Each channel has a width of 25 millimetres. The temperature distribution on the

plate will be analyzed in three layers, with distances from the bottom layer of 3.5 millimetres, 6.5 millimetres, and 9.5 millimetres, corresponding to layers 3, 2, and 1, respectively. The cooling plate exhibits uniformity diagonally. Paths will be defined to represent temperature distribution in straight lines, divided into paths 1, 2, and 3 according to the layer. These paths traverse five lines: AA-FF, A-C, F-D, a-e, and f-j.

For the cooling plate boundaries, including both the plain plate and the plate with channels shown in Figure 4, temperatures at the sides and the bottom are set to 30 degrees Celsius, the typical air temperature in Thailand. Natural convection heat transfer is assumed with a heat transfer coefficient of 20 W/m^2 K. On the top of the cooling plate, initial temperatures remain constant at 40, 50, 60, and 70 degrees Celsius, respectively. The same conditions as the plain plate are applied to the channel boundaries. However, heat transfer coefficients for the larger channels (12 channels) are set to 4200 and 3000 W/m^2 K, obtained from calculations based on Equation 1 from Dittus-Boelter [29] equation.

$$Nu = \frac{hD_h}{k} = f(\mathrm{Re}, \mathrm{Pr}) \tag{1}$$

Where Nu is the Nusselt number, h is the convective heat transfer coefficient, D_h is the hydraulic diameter of the channel, k is the thermal conductivity of the fluid, Re is the Reynolds number, Pr is the Prandtl number.

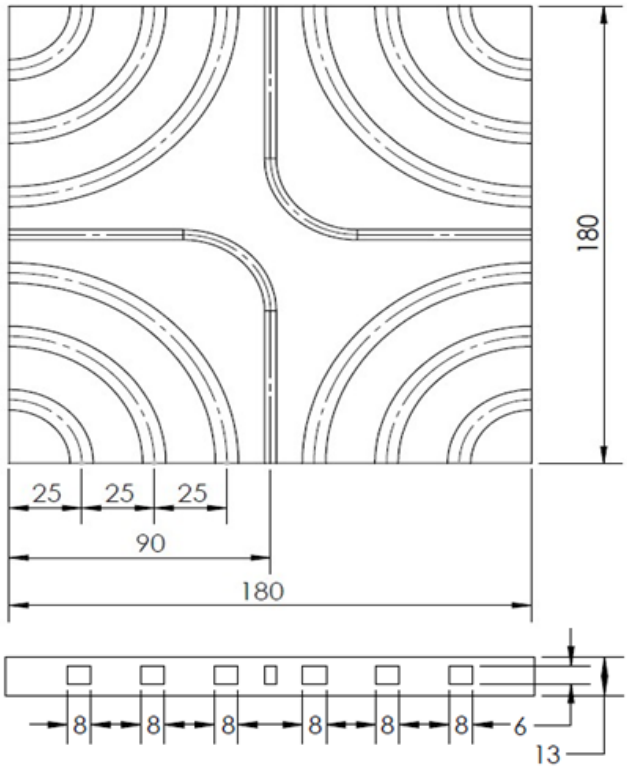

Figure 2 Geometric details

Reynolds numbers are set at 5300 and 3600, respectively. For the smaller channels (2 channels), a constant Reynolds number of 5000 is maintained, with a heat transfer coefficient of 5600 W/m2 K applied to all cases.

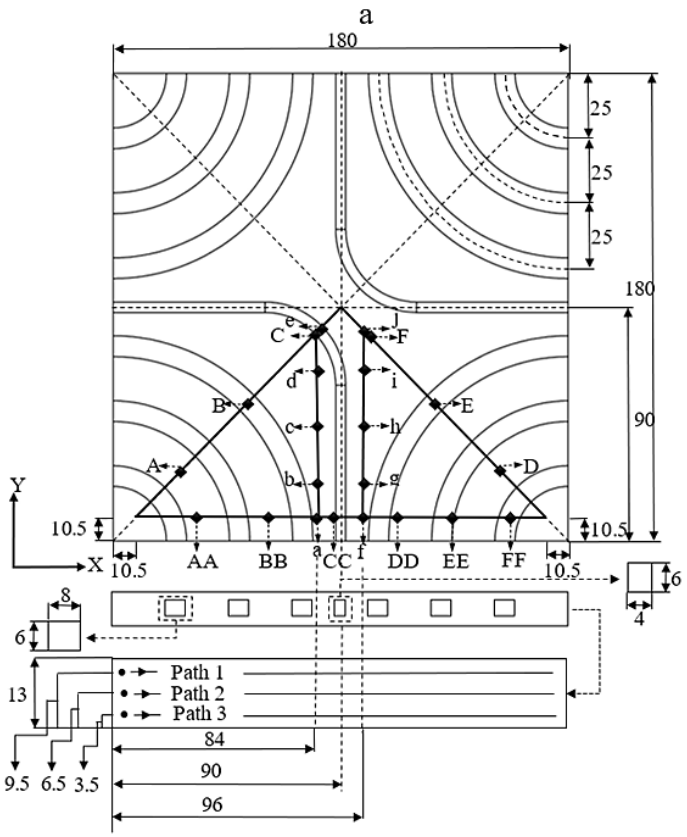

Figure 3 Path lines and positions, indicating the temperature distribution of the plate

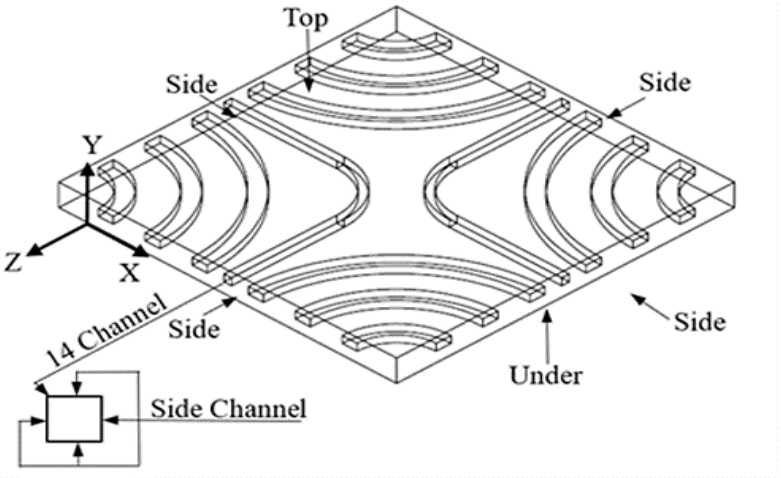

Figure 4 Defined boundary conditions.

The temperature inside the channels is set to 0 degrees Celsius in all cases. The division of mesh, grid, or elements for both the plain plate and the plate with channels, as shown in Figure 4, was carried out. Mesh independence study was conducted with four sizes: 1258, 2720, 5676, 13316, and 253589. Considering the plain plate's thermal conductivity, the percentage error was observed to be 2%, 1%, 1%, 1%, and 1%, respectively. However, the size of 13316 was selected for the plate with added channels, as depicted in Figure 4b.

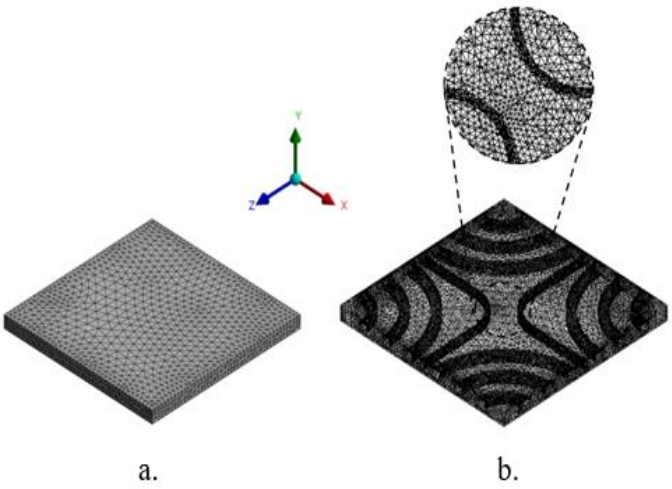

Figure 5 Grid division: a) Cooling plate b) Cooling plate with channel.

RESULTS AND DISCUSSION

The analysis of temperature distribution across cooling plates between Layers 1, 2, and 3, under the condition of setting h at the sides of the channel to h = 3000 W/m^2 and 4200 W/m^2, is shown in Figure 6. The temperature distribution exhibits a similar pattern when the temperature is set between 40-70 degrees Celsius. The central region of the plate has a higher temperature than areas with channels. Here, only the initial temperature of 40 degrees is shown, as the temperature distribution for other values follows the same pattern, as depicted in Figure 6.

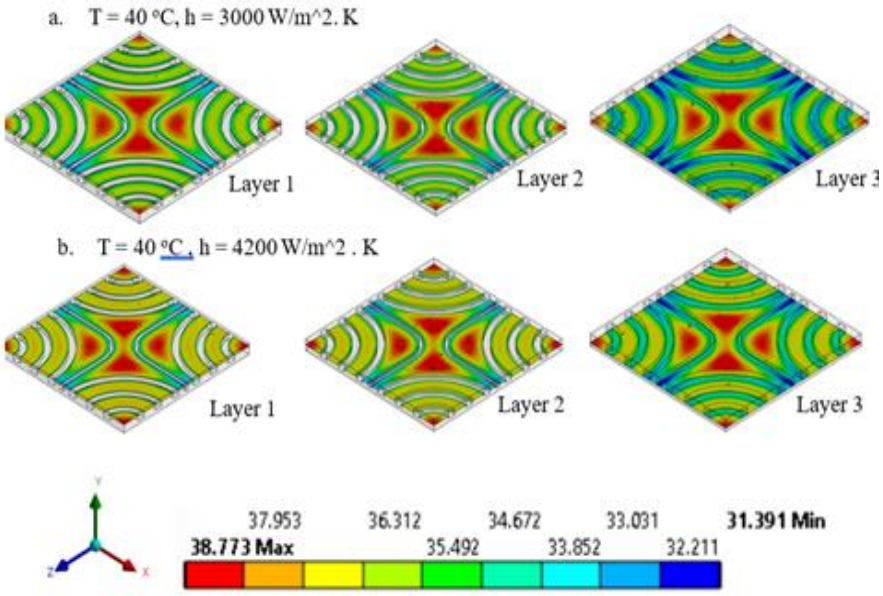

Figure 6 Temperature distribution on layers 1, 2, and 3 of the plate with an initial temperature set at the top side of the cooling plate: a) T = 40°C, h = 3000 W/m² b) T = 40°C, h = 47200 W/m²

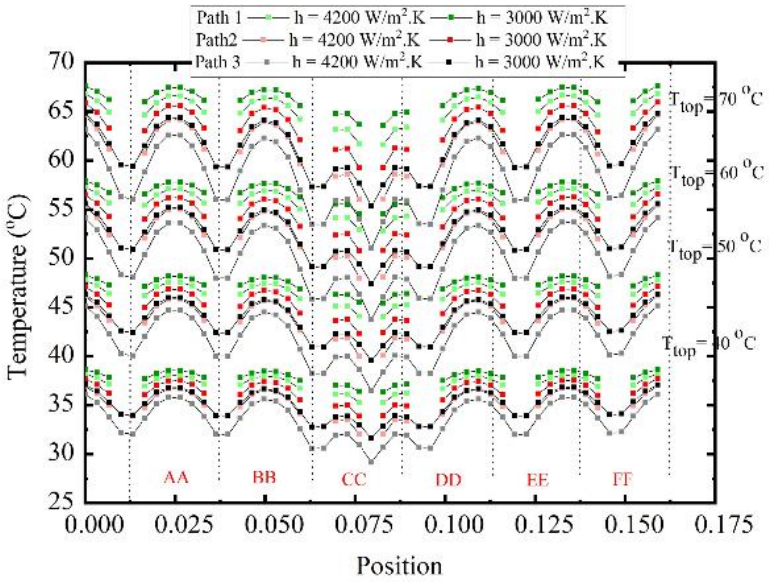

Figure 7 Values of temperature distribution along Paths 1, 2, and 3, showing positions on line AA – FF

Refer to the temperature lines shown in Figure 3 when considering the temperature distribution at various positions on the cooling plate. The analysis follows paths 1, 2, and 3, corresponding to the temperature lines AA-FF in Figure 7, a-e and f-j in Figure 8, and A-C and D-F in Figure 9.

It is crucial to note that path 1, which represents the topmost layer, exhibits temperatures that are closest to the initial temperature. Furthermore, at h = 4200 W/m^2K, the temperature distribution across all lines is consistently lower than at h = 3000 W/m^2K for the entire temperature range of 40-70°C. Figure 7 vividly illustrates the temperature distribution along the edges of the plate, indicating a relatively uniform distribution from AA to FF. In Figure 8, the temperature distribution follows a similar trend between a-e and f-j. However, the segment i-j, which contains a channel, shows a significant gap in temperature, leading to an absence of temperature values in that region.

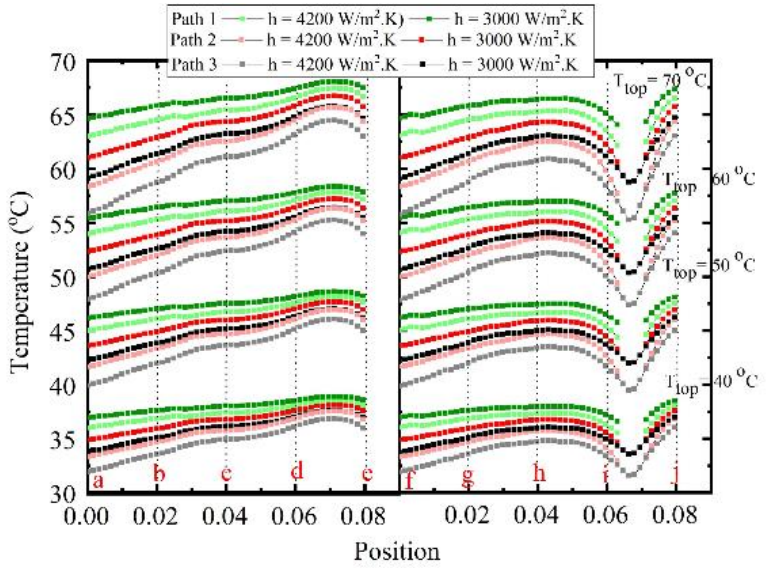

Figure 8 Values of temperature distribution along Paths 1, 2, and 3, showing positions on line a – j

Similarly, in Figure 9, the segments A-C and D-F show a similar trend. However, the middle sections B-C and E-F, located in the central region, exhibit higher temperatures closer to the initial temperature of the plate.

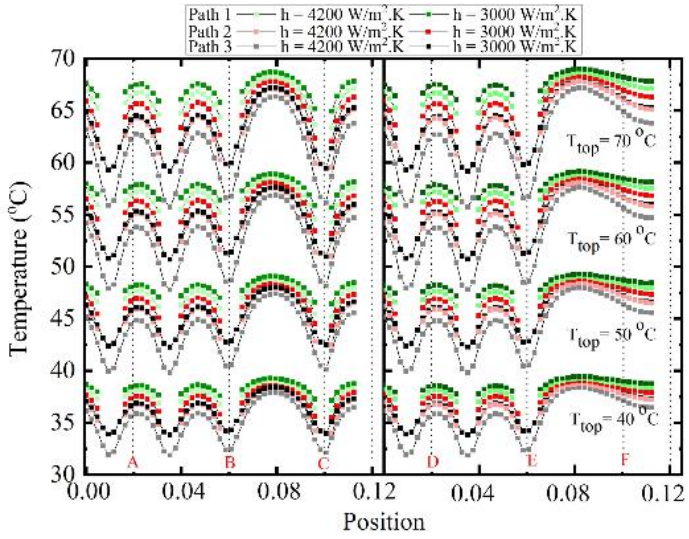

Figure 9 Values of temperature distribution along Paths 1, 2, and 3, showing positions on line A – F

When considering the heat transfer of the cooling plate at different initial temperatures, as shown in Figure 10, the heat flux ratio between the plate with channels and the plain plate is analyzed. At an initial temperature of 40 degrees Celsius, the heat flux ratio is higher compared to initial temperatures of 50, 60, and 70 degrees Celsius. This pattern is consistent for both cases where h = 3000 W/m^2K and h = 4200 W/m^2K. Higher h values result in a higher heat flux ratio. Additionally, at an initial temperature of 70 degrees Celsius, the heat flux ratios for h = 3000 W/m^2K and h = 4200 W/m^2K are very similar.

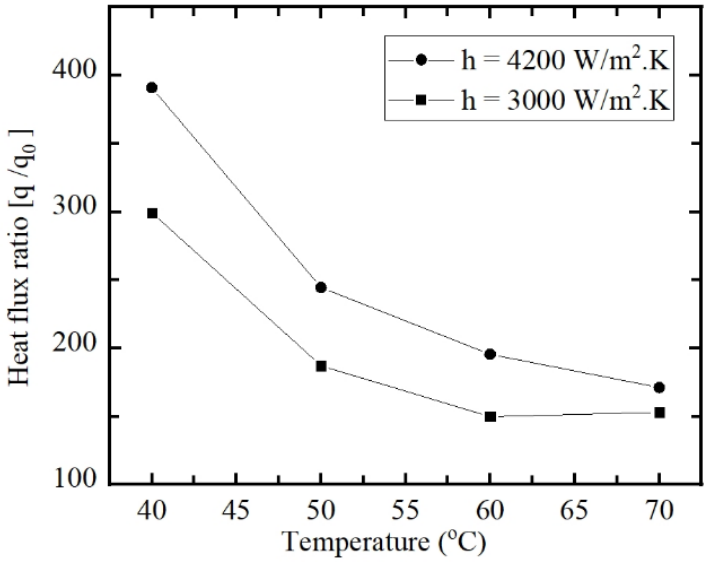

Figure 10 The heat flux ratio of the cooling plate with channels compared to the plain cooling plate, with different initial temperatures and values of h = 3000 W/m² and h = 4200 W/m², respectively.

CONCLUSION

This research studies the design of cooling plate channels by varying the heat transfer coefficient (h) within the channels. It was found that a higher h results in better temperature and heat distribution compared to a lower h. Furthermore, as the initial temperature increases, the difference in heat transfer between different h values becomes negligible. The central region of the plate is less affected by the lower temperatures within the channels. These findings can be helpful for future arrangements of battery modules.

Acknowledgements

We are grateful for Suranaree University of Technology (SUT) 's financial support through the OROG (One Research One Graduate) program.

REFERENCES

[1] X. Li, F. He, and L. Ma, "Thermal management of cylindrical batteries investigated using wind tunnel testing and computational fluid dynamics simulation," Journal of Power Sources, vol. 238, 15 September 2013, pp. 395–402.

[2] G. Miranda and C. W. Hong, "Integrated modeling for the cyclic behavior of high power Li-ion batteries under extended operating conditions," Applied Energy, Vol. 111, November 2013, pp. 681–689.

[3] X. Feng, et al., "Thermal runaway mechanism of lithium ion battery for electric vehicles: A review," Energy Storage Materials, Vol. 10, January 2018, pp. 246–267.

[4] F. Zhang, et al., "Propagation dynamics of the thermal runaway front in large-scale lithium-ion batteries: Theoretical and experiment validation," International Journal of Heat and Mass Transfer, Vol. 225(15), 15 June 2024, pp. 125393.

[5] K. Abhilash, A. Jadhav, et al., "Numerical study on thermal runaway in a cell and battery pack at critical heating conditions with variation in heating powers," Journal of Energy Storage, Vol. 90, 15 June 2024, pp. 111813.

[6] H. Wang, Q. Wang, Z. Zhao, et al., "Thermal runaway propagation behavior of the cell-to-pack battery system," Journal of Energy Chemistry, Vol. 84, September 2023, pp.162–172.

[7] Z. Wencan, L. Zhicheng, Y. Xiuxing, et al., "Avoiding thermal runaway propagation of lithium-ion battery modules by using hybrid phase change material and liquid cooling," Applied Thermal Engineering, Vol. 184, 5 February 2021, pp.116380.

[8] S. A. Bonab, S. A. Zonouzi, H. Aminfar, "Combination of flow boiling cooling by taking advantage of helical pipes and air cooling for thermal management of lithium-ion batteries," Journal of Energy Storage, Vol. 72, 15 November 2023, pp. 108322.

[9] S. P. Verma, S. Saraswati, "Comprehensive thermal performance analysis of an air-cooled staggered configured Li-ion battery pack- A numerical and experimental approach," Journal of Energy Storage, Vol. 89, 1 June 2024, pp. 111792.

[10] S. Amosedinakaran, R. Kannan, S. Kannan, et al., "Performance Analysis for Battery Stability Improvement using Direct Air Cooling Mechanism for Electric Vehicles," e-Prime - Advances in Electrical Engineering, Electronics and Energy, Vol. 8, June 2024, pp. 100585.

[11] S. P. Verma, S. Saraswati, "Numerical and experimental analysis of air-cooled Lithium-ion battery pack for the evaluation of the thermal performance enhancement," Journal of Energy Storage, Vol. 73, 10 December 2023, pp. 108983.

[12] M. Li, S. Ma, H. Jin, et al., "Performance analysis of liquid cooling battery thermal management system in different cooling cases," Journal of Energy Storage, Vol. 72, 30 November 2023, pp.108651.

[13] N. Wu, Y. Chen, B. Lin, et al., "Experimental assessment and comparison of single phase versus two-phase liquid cooling battery thermal management systems," Journal of Energy Storage, Vol. 72, 30 November 2023, pp. 108727.

[14] D. Zhao, C. An, Z. Jia, et al., "Structure optimization of liquid-cooled plate for electric vehicle lithium-ion power batteries," International Journal of Thermal Sciences, Vol.195, January 2024, pp. 108614.

[15] Y. Zhang, W. Zuo, E. Jiaqiang, et al., "Performance comparison between straight channel cold plate and inclined channel cold plate for thermal management of a prismatic LiFePO4 battery," Energy, Vol. 248, 1 June 2022, pp. 123637.

[16] R. Kumar, V. Goel, "A study on thermal management system of lithium-ion batteries for electrical vehicles: A critical review," Journal of Energy Storage, Vol. 71, 1 November 2023 pp. 108025.

[17] S. Panchal, I. Dincer, M. Agelin-Chaab, et al., "Thermal modeling and validation of temperature distributions in a prismatic lithium-ion battery at different discharge rates and varying boundary conditions," Applied Thermal Engineering, Vol. 96, 5 March 2016, pp.190–199.

[18] M. A. Alghassab, "Investigating the performance improvement of lithium-ion battery cooling process using copper fins and phase change materials (PCMs)," Case Studies in Thermal Engineering, Vol. 59, July 2024, pp. 104473.

[19] N. Putra, A. F. Sandi, B. Ariantara, et al., "Performance of beeswax phase change material (PCM) and heat pipe as passive battery cooling system for electric vehicles," Case Studies in Thermal Engineering, Vol. 21, October 2020, pp. 100655.

[20] M. Luo, Y. Zhang, Z. Wang, et al., "Thermal performance enhancement with snowflake fins and liquid cooling in PCM-based battery thermal management system at high ambient temperature and high discharge rate," Journal of Energy Storage, Vol. 90, 15 June 2024, pp. 111754.

[21] Z. Liu, B. Wang, Y. Tan, P. Li, "Thermal management of lithium-ion battery pack under demanding conditions and long operating cycles using fin-enhanced PCMs/water hybrid cooling system," Applied Thermal Engineering, Vol. 233, October 2023, pp. 121214.

[22] X.K. Yu, Y.B. Tao, Q.Q. Deng, "Experimental study on thermal management of batteries based on the coupling of metal foam-paraffin composite phase change materials and air cooling," Journal of Energy Storage, Vol. 84, 20 April 2024, pp. 110891.

[23] Z. Chen, X. Hong, Z. Huo, "Enhancing lithium-ion battery cooling efficiency through leaf vein-inspired double-layer liquid cooling plate design," Journal of Energy Storage, Vol. 88, 30 May 2024, pp. 111584.

[24] P. He, H. Lu, et al., "Numerical investigation on a lithium-ion battery thermal management system utilizing a double-layered I-shaped channel liquid cooling plate exchanger," International Journal of Thermal Sciences, Vol. 187, May 2023, pp. 108200.

[25] D. Zhao, Z. Lei, C. An, "Research on battery thermal management system based on liquid cooling plate with honeycomb-like flow channel," Applied Thermal Engineering, Vol. 218, 5 January 2023, pp. 119324.

[26] K. Kirad, M. Chaudhari, "Design of cell spacing in lithium-ion battery module for improvement in cooling performance of the battery thermal management system," Journal of Power Sources, Vol. 481 1 January 2021, pp. 229016.

[27] Y. Lia, Z. Zhoub, W.T. Wu, "Three-dimensional thermal modeling of Li-ion battery cell and 50 V Li-ion battery pack cooled by mini-channel cold plate," Applied Thermal Engineering, Vol. 147, 25 January 2019, pp. 829-840.

[28] W. Kong, C. Zhang, Z. Ji, "Investigation on the cooling effect of a novel composite channel cold plate for lithium-ion battery," Journal of Energy Storage, Vol. 86, 1 May 2024, pp. 111183.

[29] Y. A. Cengel, A. J. Ghajar, "Heat and mass transfer," fundamentals & applications, New York, 2015.